

---

# Self-supervised Pre-training for Precipitation Post-processor

---

**Sojung An\***<sup>†</sup>  
KIAPS

Seoul, Republic of Korea  
sojungan@kiaps.org

**Junha Lee\***  
KITECH

Ansan, Republic of Korea  
junha@kitech.re.kr

**Jiyeon Jang**  
KIAPS

Seoul, Republic of Korea  
jyjang@kiaps.org

**Inchae Na**  
KIAPS

Seoul, Republic of Korea  
icna@kiaps.org

**Wooyeon Park**  
KIAPS

Seoul, Republic of Korea  
wooyeon@kiaps.org

**Sujeong You**  
KITECH

Ansan, Republic of Korea  
sjyou21@kitech.re.kr

## Abstract

Securing sufficient forecast lead time for local precipitation is essential for preventing hazardous weather events. Nonetheless, global warming-induced climate change is adding to the challenge of accurately predicting severe precipitation events, such as heavy rainfall. In this work, we propose a deep learning-based precipitation post-processor approach to numerical weather prediction (NWP) models. The precipitation post-processor consists of (i) self-supervised pre-training, where parameters of encoder are pre-trained on the reconstruction of masked variables of the atmospheric physics domain, and (ii) transfer learning on precipitation segmentation tasks (target domain) from the pre-trained encoder. We also introduce a heuristic labeling approach for effectively training class-imbalanced datasets. Our experiment results in precipitation correction for regional NWP show that the proposed method outperforms other approaches.

## 1 Introduction

Precipitation forecasting plays a vital role in weather science, holding significant importance in our comprehension and readiness for meteorological phenomena. Deep learning has been rapidly adopted in precipitation forecasting, such as simulating echo movement and predicting typhoon trajectories based on observation data [20, 21, 17, 1]. However, relying exclusively on observational data fails to capture the fundamental physical and dynamic mechanisms in the real world, resulting in an exponential increase in error as the forecast lead time increases [3]. In addition, climate change increases the uncertainty of predicting extreme events such as torrential rains [15]. Limited forecast lead time makes it difficult for infrastructure to prepare in advance for extreme weather events.

Recent research is actively conducted to enhance forecast lead times through post-processing NWP model data [11, 6, 18, 25]. Espeholt et al. [3] proposed Metnet2, a 12-hour probabilistic forecasting model, by designing a hybrid model consisting of a forecasting model based on observation data and a post-processing NWP model data. While Metnet2 displayed promising results, simulating heavy rainfall remains a challenging task.

Therefore, we designed a self-supervised pre-training process that takes into account the physical and dynamic processes among atmospheric variables to improve the relative bias and reliability of

---

\*These authors contributed equally to this work.

<sup>†</sup>Corresponding author

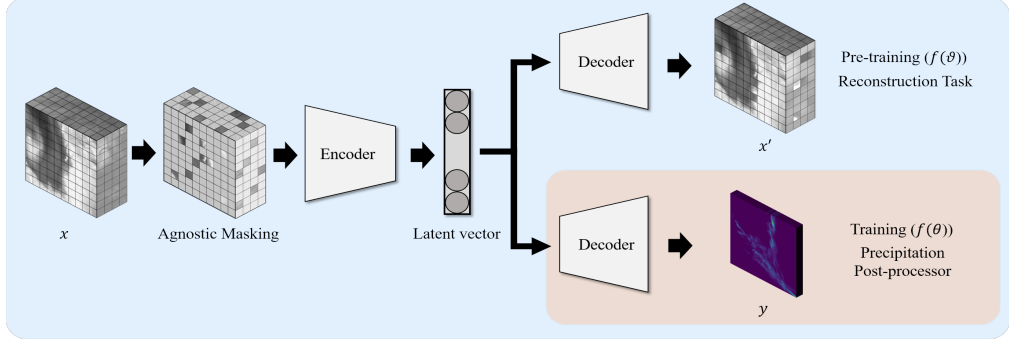


Figure 1: Process flow of learning the precipitation post-processor. The model consists of two main phases: 1) pre-training the encoder and decoder by a reconstruction task after masking the inputs; 2) training the decoder for precipitation prediction using the trained encoder. The latent vector learned during pre-training is used as an encoder with fixed weights during main training.

heavy rain prediction performance. To this aim, we randomly mask three-dimensional images [5] and train an encoder-decoder to reconstruct the variables based on dynamic sparse kernels (DSKs) [23]. Afterward, we train a decoder for probability-based precipitation correction based on the pre-trained encoder. The pre-training process is advantageous for correlation analysis based on NWP model variables and provides additional data augmentation effects. We propose a continuous labeling method for learning on class-imbalanced datasets that facilitates a continuous probability distribution based on precipitation density.

## 2 Method

In this section, we present in detail our proposed approach. We commence with a self-supervised pre-training procedure aimed at formulating the reconstruction task. Subsequently, we describe our target process for precipitation post-processing.

### 2.1 Problem formulation

Given a set of ground-truth pairs  $\mathbf{G} = (\{x_i\}_1^n, \{y_j\}_1^c)$  with  $x \in \mathbb{R}^{n \times h \times w}$ ,  $y \in \mathbb{R}^{c \times h \times w}$ , and  $z \in \mathbb{R}^d$ , we denote input  $x = \{x_1, \dots, x_n\}^T$ , and output  $y = \{y_1, \dots, y_c\}^T$ . Our goal is to precipitation segmentation function  $f : \mathbb{R}^d \rightarrow \mathbb{R}^c$ , assuming  $z \in \mathbb{R}^d$  be a latent space with distribution  $p(z)$  by the pre-training process. We set reconstruction task  $f'_\theta$  of NWP data to predict our target object function  $f_\theta$ . The probabilistic encoder-decoder of the proposed method is defined as:

$$\mathcal{L}(\theta, \vartheta; x) = -\frac{1}{2} \mathbb{E}_{q_\vartheta(z|x)} [||x - \hat{x}||_{L_2}] + \text{KL}(q_\vartheta(z|x); p^*(z)), \quad (1)$$

where  $q_\vartheta$  is the pre-training process distribution and  $p^*$  is class-probability distribution. Mean squared error loss function is used to minimize pre-training loss. The training component is the KL Divergence term, which quantifies the difference between the distribution of the latent variables, denoted as  $z$ , learned by our encoded as  $q_\vartheta(z|x)$ , and a prior distribution denoted as  $p(z)$ .

### 2.2 Continuous labeling

In multi-class classification according to ranges of precipitation intensity, we seek to classify instances  $x$  into one of labels  $y$ . Let  $p^*(x) = [\mathbb{P}(y|z)]$  is the class-probability distribution and  $\mathcal{L}$  is the cross-entropy loss,  $\mathcal{F}$  is computed as follow:

$$\mathcal{F} = \mathbb{R}[p^*(x)^T \mathcal{L}(f(x))] = \frac{1}{c} \sum_{i=1}^c w_i \cdot \hat{y}_i^T \mathcal{L}(f(x_i)), \quad (2)$$

where  $w_y$  refers to the weight set according to labels and  $\hat{y}$  denotes the stochastic labeling. The minimization leads to the maximum likelihood estimate of the classifier parameters. Unlike one-hot

labeling, where the probability takes a value of 1, the method for smoothing the probability values based on the density of the label range is described in algorithm 1.

---

**Algorithm 1:** Continuous labeling on density of rainfall range

---

**Input:** QPE  $\mu = [0, 100]$ ; rainfall threshold set  $\gamma = \{r_0, \dots, r_{n-1}\}$   
**Output:** probability label  $\hat{Y}$

```

1 Initialize the number of rainfall threshold  $n$ 
2  $p(y_i) = \begin{cases} 1, & \text{if } r_i \leq \mu < r_{i+1} \quad /* \text{ Set the probability of label } i \text{ to 1. */} \\ 0, & \text{otherwise} \quad /* \text{ Set probability of 0 for label } i \text{ if outside range. */} \end{cases}$ 
3 while  $i$  do
4   switch  $p(y_i)$  do
5     if  $\{x \leq r_{i-1}\}$   $p^*(y_i) \rightarrow 0$ 
6     else if  $\{r_{i-1} < x \leq r_i\}$   $p^*(y_i) \rightarrow \frac{r_{i+1}-x}{r_{i+1}-r_i}$ 
7     else if  $\{r_i < x \leq r_{i+1}\}$   $p^*(y_i) \rightarrow 1 - \frac{x-r_i}{r_i-r_{i-1}}$ 
8     else if  $\{i = n-1\}$   $p^*(y) \rightarrow 1$ 
9     else  $\Rightarrow p^*(y) \rightarrow 0$ 
10   end
11 end
12 return  $p(y), p^*(y)$ 

```

---

### 2.3 Training model

In this section, we present our post-processing method that perturbs a whole patch to the reconstruction task with InternImage [23] as an encoder and UPerNet [24] as a decoder.

**Patch embedding.** We tokenize the input data into non-overlapping spatial-temporal patches [4]. Each 3D patch has dimensions  $\mathcal{M} \in \mathbb{R}^{t \times p \times p}$ , and this patchify results in  $x \in \mathbb{R}^{c/4 \times h/p \times w/p}$  tockens. We then flatten the data and transform the tokens into  $x \in \mathbb{R}^{chw/4p^2 \times c}$  through a projection process. The data adds spatio-temporal positional encoding that follows the same size.

**Masking.** We use a structure-agnostic sample strategy for masking the patches randomly without replacement from the set of embedded patches using [5]. For a pre-training model with a reconstruction task, the optimal masking ratio is related to how much information is redundant in the data [2, 8]. In the case of numerical forecasting models, there is similar information redundancy as each weather variable is for the same point in time, but each variable has its own physical information. Following the hypothesis, our masking ratio is determined based on empirical results. Masking ratio of pre-training and training is set to 90% and 25%, respectively. The masked patches undergo layer normalization and restore to their original input dimensions  $x' \in \mathbb{R}^{c \times h \times w}$ .

**Encoder and decoder.** We utilize DSK layers in InternImage [23] as an encoder for adaptive spatial aggregation conditioned. InternImage is a backbone model that achieves effects beyond attention in the receptive field required for downstream tasks. By applying each encoder layers,  $e_i \subset e$ , that are stacked to hierarchy hidden states  $h_i \in \mathbb{R}^{ic \times h/i \times w/i}$ . We train the ability to effectively segment while preserving object boundaries and details from the training data using the UperNet decoder.

## 3 Experiments

We classified rainfall up to  $[0, 0.1)$  as no rain,  $[0.1, 10)$  as rain, and above 10 mm as heavy rain. Figure 2 shows a breakdown of the proportion of each labeling. The proportion of heavy rain within the training dataset is approximately 0.75%, indicating a significant data imbalance. The class imbalance issue frequently encountered in precipitation measurement data poses a common challenge in precipitation forecasts. Therefore, we investigate how the proposed method tackles class imbalance issues during the model

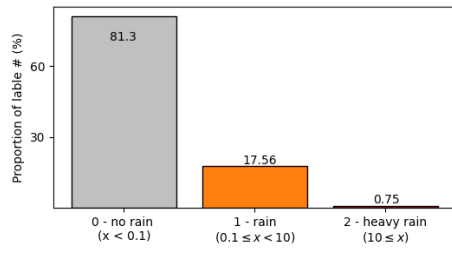


Figure 2: Visualization for the proportion of labels of training dataset.

Table 1: Summary of results for our tasks.  $\mathcal{I}$ ,  $p^*$ , and  $\vartheta$  denote the InternImage, label smoothing, and transfer learning, respectively. The comparative tables are presented to results of the models with threshold 0.1 mm, and 10 mm.

Method	0.1 mm $\uparrow$				10 mm $\uparrow$			
	CSI	F1	Precision	Recall	CSI	F1	Precision	Recall
RDAPS	0.296	0.456	0.405	0.522	0.062	0.117	0.077	<b>0.238</b>
Metnet	0.276	0.433	0.427	0.439	0.007	0.015	0.015	0.274
Metnet+ $p^*$	0.271	0.427	0.390	0.472	0.057	0.107	0.002	0.275
$\mathcal{I}+p^*$	0.316	0.488	0.488	0.502	0.017	0.020	0.020	0.132
$\mathcal{I}+\vartheta$	0.329	0.443	0.443	<b>0.523</b>	0.060	0.076	0.075	0.222
$\mathcal{I}+p^*+\vartheta$ (ours)	<b>0.347</b>	<b>0.515</b>	<b>0.620</b>	0.481	<b>0.093</b>	<b>0.169</b>	<b>0.130</b>	0.227

training process. We compare and evaluate our post-processor and heuristic label approach against the state-of-the-art precipitation forecasting model called Metnet. Our main results are summarized in Table 1 and Figure 3. These results show the performance of the proposed methods, precipitation post-processor, a prior method based on self-supervised learning, and baseline in the continuous smoothing settings discussed previously, where we must learn from: (i) solving the unbalanced label, and (ii) obtained connection among the variables from the self-supervised learning.

The model was trained using continuous labeling, as demonstrated in Section 2.2, and this approach had a noticeable impact on performance improvement. We observed a significant enhancement in precipitation forecasting accuracy exceeding 10mm when employing continuous labeling in MetNet. In Figure 3, we observe that precipitation above 10 mm covers a large part of the Korean Peninsula, while NWP underestimates it. On the other hand, a deep learning-based post-processing model can capture signals above 10 mm. The limitation lies in the fact that the input data relies on NWP predictions rather than observations, and as a result, it can only be learned with some degree of error.

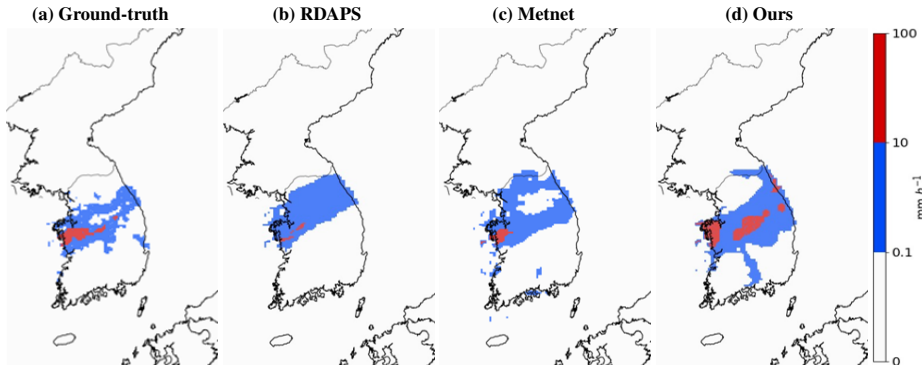


Figure 3: Qualitative comparison between models on August 10 2022 at 00 UTC. Each result represents a cumulative result over a one-hour period. Due to the influence of the stagnant front, rain fell in most parts of the Korea, the average rainfall is 100~200 mm in a day, and the maximum is more than 300 mm.

## 4 Conclusion

In this work, we propose a novel approach for precipitation post-processor based on transfer learning for target domain adaptation with two main contributions: 1) applying the transfer learning to the atmosphere system, by pre-training on the reconstruction domain and integrating the parameters in the segmentation domain; and 2) stochastic softening one-hot labeling to overcome bias learning from unbalanced data. We showed through empirical results on domain adaptation from the two-step training strategy that the proposed method helps understand the correlation among atmospheric variables, yielding better transfer learning performances on precipitation post-processor.

## References

- [1] Sojung An. Nowcast-to-forecast: Token-based multiple remote sensing data fusion for precipitation forecast. In *Proceedings of the 32nd ACM International Conference on Information and Knowledge Management*, 2023.
- [2] Jacob Devlin, Ming-Wei Chang, Kenton Lee, and Kristina Toutanova. Bert: Pre-training of deep bidirectional transformers for language understanding. *arXiv preprint arXiv:1810.04805*, 2018.
- [3] Lasse Espeholt, Shreya Agrawal, Casper Sønderby, Manoj Kumar, Jonathan Heek, Carla Bromberg, Cenk Gazen, Rob Carver, Marcin Andrychowicz, Jason Hickey, et al. Deep learning for twelve hour precipitation forecasts. *Nature communications*, 13(1):1–10, 2022.
- [4] Haoqi Fan, Bo Xiong, Karttikeya Mangalam, Yanghao Li, Zhicheng Yan, Jitendra Malik, and Christoph Feichtenhofer. Multiscale vision transformers. In *Proceedings of the IEEE/CVF international conference on computer vision*, pages 6824–6835, 2021.
- [5] Christoph Feichtenhofer, Yanghao Li, Kaiming He, et al. Masked autoencoders as spatiotemporal learners. *Advances in neural information processing systems*, 35:35946–35958, 2022.
- [6] Mohammadvaghef Ghazvinian, Yu Zhang, Dong-Jun Seo, Minxue He, and Nelun Fernando. A novel hybrid artificial neural network-parametric scheme for postprocessing medium-range precipitation forecasts. *Advances in Water Resources*, 151:103907, 2021.
- [7] Priya Goyal, Piotr Dollár, Ross Girshick, Pieter Noordhuis, Lukasz Wesolowski, Aapo Kyrola, Andrew Tulloch, Yangqing Jia, and Kaiming He. Accurate, large minibatch sgd: Training imagenet in 1 hour. *arXiv preprint arXiv:1706.02677*, 2017.
- [8] Kaiming He, Xinlei Chen, Saining Xie, Yanghao Li, Piotr Dollár, and Ross Girshick. Masked autoencoders are scalable vision learners. In *Proceedings of the IEEE/CVF conference on computer vision and pattern recognition*, pages 16000–16009, 2022.
- [9] Ryan Keisler. Forecasting global weather with graph neural networks. *arXiv preprint arXiv:2202.07575*, 2022.
- [10] Ki-Hwan Kim, Pyoung-Seop Shim, and Seoleun Shin. An alternative bilinear interpolation method between spherical grids. *Atmosphere*, 10(3):123, 2019.
- [11] Taehyeon Kim, Namgyu Ho, Donggyu Kim, and Se-Young Yun. Benchmark dataset for precipitation forecasting by post-processing the numerical weather prediction. *arXiv preprint arXiv:2206.15241*, 2022.
- [12] Ilya Loshchilov and Frank Hutter. Sgdr: Stochastic gradient descent with warm restarts. *arXiv preprint arXiv:1608.03983*, 2016.
- [13] Ilya Loshchilov and Frank Hutter. Decoupled weight decay regularization. *arXiv preprint arXiv:1711.05101*, 2017.
- [14] Xin Man, Chenghong Zhang, Changyu Li, and Jie Shao. W-mae: Pre-trained weather model with masked autoencoder for multi-variable weather forecasting. *arXiv preprint arXiv:2304.08754*, 2023.
- [15] Katrin M Nissen and Uwe Ulbrich. Increasing frequencies and changing characteristics of heavy precipitation events threatening infrastructure in europe under climate change. *Natural Hazards and Earth System Sciences*, 17(7):1177–1190, 2017.
- [16] Jaideep Pathak, Shashank Subramanian, Peter Harrington, Sanjeev Raja, Ashesh Chattopadhyay, Morteza Mardani, Thorsten Kurth, David Hall, Zongyi Li, Kamyar Azizzadenesheli, et al. Fourcastnet: A global data-driven high-resolution weather model using adaptive fourier neural operators. *arXiv preprint arXiv:2202.11214*, 2022.
- [17] Suman Ravuri and Oriol Vinyals. Classification accuracy score for conditional generative models. *Advances in neural information processing systems*, 32, 2019.

- [18] Adrian Rojas-Campos, Martin Wittenbrink, Pascal Nieters, Erik J Schaffernicht, Jan D Keller, and Gordon Pipa. Postprocessing of nwp precipitation forecasts using deep learning. *Weather and Forecasting*, 38(3):487–497, 2023.
- [19] Ramprasaath R Selvaraju, Michael Cogswell, Abhishek Das, Ramakrishna Vedantam, Devi Parikh, and Dhruv Batra. Grad-cam: Visual explanations from deep networks via gradient-based localization. In *Proceedings of the IEEE international conference on computer vision*, pages 618–626, 2017.
- [20] Xingjian Shi, Zhourong Chen, Hao Wang, Dit-Yan Yeung, Wai-Kin Wong, and Wang-chun Woo. Convolutional lstm network: A machine learning approach for precipitation nowcasting. *Advances in neural information processing systems*, 28, 2015.
- [21] Xingjian Shi, Zhihan Gao, Leonard Lausen, Hao Wang, Dit-Yan Yeung, Wai-kin Wong, and Wang-chun Woo. Deep learning for precipitation nowcasting: A benchmark and a new model. *Advances in neural information processing systems*, 30, 2017.
- [22] Casper Kaae Sønderby, Lasse Espeholt, Jonathan Heek, Mostafa Dehghani, Avital Oliver, Tim Salimans, Shreya Agrawal, Jason Hickey, and Nal Kalchbrenner. Metnet: A neural weather model for precipitation forecasting. *arXiv preprint arXiv:2003.12140*, 2020.
- [23] Wenhui Wang, Jifeng Dai, Zhe Chen, Zhenhang Huang, Zhiqi Li, Xizhou Zhu, Xiaowei Hu, Tong Lu, Lewei Lu, Hongsheng Li, et al. Internimage: Exploring large-scale vision foundation models with deformable convolutions. In *Proceedings of the IEEE/CVF Conference on Computer Vision and Pattern Recognition*, pages 14408–14419, 2023.
- [24] Tete Xiao, Yingcheng Liu, Bolei Zhou, Yuning Jiang, and Jian Sun. Unified perceptual parsing for scene understanding. In *Proceedings of the European conference on computer vision (ECCV)*, pages 418–434, 2018.
- [25] Yuhang Zhang and Aizhong Ye. Machine learning for precipitation forecasts postprocessing: Multimodel comparison and experimental investigation. *Journal of Hydrometeorology*, 22(11):3065–3085, 2021.
- [26] Bolei Zhou, Aditya Khosla, Agata Lapedriza, Aude Oliva, and Antonio Torralba. Learning deep features for discriminative localization. In *Proceedings of the IEEE conference on computer vision and pattern recognition*, pages 2921–2929, 2016.

## A Data

In this study, we extracted regional data assimilation and prediction system integrated model (RDAPS-KIM) data for lead time from 25 hours to 30 hours at 1-hour intervals. For NWP models, it takes about 6 hours to generate a forecast field through data assimilation, so we extracted data from 25 to 30 hours for a 24-hour forecast. The RDAPS-KIM is organized into a domain with a resolution of 3 km covering the East Asia region. The variables were empirically selected based on previous studies [16, 14, 9], as shown in 2.

Table 2: Summary of datasets used in input data. The data consists of 16 variables as input. We use seven physical variables with 4 pressure levels: temperature (T),  $U$ -component of the wind speed (U),  $V$ -component of the wind speed (V), geopotential height (Z), relative humidity (RH), sea level pressure (SLP), and rain.

Vertical Level	Variables
Surface	$U_{10}, V_{10}, T_2, SLP, rain$
850hPa	$U, V, T, Z, RH$
500hPa	$U, V, T, Z, RH$
100hPa	Z

### A.1 Ground-truth data

Quantitative Precipitation Estimation (QPE), a reanalysis dataset for the Korean Peninsula region, is used as the ground truth data. The data is composed of data with a 5 km resolution at 1-hour intervals and covers approximately a longitude of 149 to a latitude of 253. The QPE is a data set adjusted to the nearest natural rainfall by combining ground observations from AWS and SHK060, radar data, and satellite data.

The spatial resolution of the regional forecast model (UM 12kmL70) is 12 km, and it is vertically composed of 70 layers, extending up to approximately 80 kilometers. It receives boundary fields from the global forecast model at 3-hour intervals and conducts 87-hour predictions four times a day (00, 06, 12, 18UTC). The regional forecast model operates on a 6-hourly analysis-forecast cycle and utilizes the Hybrid sigma-pressure vertical coordinate along with the Arakawa C-grid staggering grid system.

## B Evaluating Metrics

There are several metrics for evaluating precipitation prediction models, and all the algorithms are evaluated following four standard ones among the metrics. The critical success index (CSI) is calculated as follows:  $CSI = \frac{TP}{TP+FP+FN}$ , where TP represents true positives, FP represents false positives, and FN represents false negatives between  $f_i^\theta$  and  $p_i^\theta$ . The  $x^\theta$  defined by the 0 or 1 according to a threshold  $x_i^\theta = \begin{cases} 1, & \text{if } x \geq \theta \\ 0, & \text{otherwise} \end{cases}$ . CSI is commonly used in precipitation forecasting tasks and measures the number of correct forecasts divided by the number of occasions. The CSI is calculated as  $\frac{TP}{TP+FP+FN}$ , where TP represents true positives, FP represents false positives, and FN represents false negatives between  $f_i^\theta$  and  $p_i^\theta$ . Precision represents the percentage of correctly predicted positive samples and is calculated as follows:  $\frac{TP}{TP+TN}$ . recall is determined by dividing the number of hits by the sum of the TP and false FN, represented as  $\frac{TP}{TP+FN}$ . F1 score is a metric that combines both precision and recall to provide a single numerical value for evaluating the performance of a classification model. The F1 score is computed as  $F1 Score = 2 \frac{Precision*Recall}{Precision+Recall}$ .

## C Implementation

**Data pre-processing.** The data used spans from June 2020 to May 2022, with September 2022 data serving as validation and August 2022 data used as the testing dataset. The model was trained on data

from June 2020 to May 2022 for pre-training, excluding the winter season and the validation and test datasets. During training, only data containing precipitation was used for training to ensure stability. For model training, we utilized the cell-linked list method to remap RDAPS data at a 3 km resolution to QPE data at a 5 km resolution [10]. All variables were normalized using z-scores. Additionally, for variables with the same attributes but different vertical level, we applied separate normalization. We extracted data for the Korean Peninsula only, resizing it to dimensions of  $224 \times 128$ .

**Metnet.** Sonderby et al. (2020) proposed a Metnet [22] for precipitation nowcasting that uses a ConvLSTM with attention mechanism. Moreover, Kim et al. (2022) uses the Metnet for the precipitation post-processor [11], which outperformed compared with other architectures. We used the architecture of themetnet, which is proposed as a precipitation post-processor. The code and data are publicly available <https://github.com/osilab-kaist/KoMet-Benchmark-Dataset>. for model validation, setting the window size to 3 and the learning rate to 3e-03. The optimizer is AdamW [13] with  $\beta_1$  and  $\beta_2$  set to 0.9 and 0.999.5

**Ours.** Our encoder is InternImage [23] architectures. Our model uses the spatial-temporal masking method. We set a spatial patch size of  $16 \times 16$  and a temporal patch size of  $4 \times 4$ . We set the loss weight of cross-entropy  $w_i = 1, 5, 10$ . For a  $16 \times 224 \times 128$  input, this patch size produces  $4 \times 14 \times 8$ . Our pre-training configuration mostly follows [23]. The specific configuration is described Table 3.

Table 3: Hyperparameters setting.

Config	Pre-training	Training
optimizer	AdamW [13]	AdamW [13]
optimizer momentum	$\beta_1, \beta_2=0.9, 0.95$	$\beta_1, \beta_2=0.9, 0.999$
weight decay	0.05	-
learning rate	1.6e-3	1e-4
learning rate schedule	cosine decay [12]	-
warmup epochs [7]	120	-
epochs	1000	200
batch size	64	32
gradient clipping	0.02	-

## D Additional Experimental Results

### D.1 Ablation on mask ratio

To find the optimal masking ratio for precipitation correction, we compared the results of the masking ratio during pre-training and transfer-learning. The results in Tables 4 and D.1 show that the larger the masking ratio in pre-training, the better the results, while the smaller the masking ratio in transfer-learning, the better the results.

Table 4: Results on mask sampling in pre-training.

Mask ratio	CSI (0.1)	CSI (10)
50%	0.310	0.088
75%	0.320	<b>0.090</b>
90%	<b>0.322</b>	0.089

Table 5: Results on mask sampling in transfer learning.

Mask ratio	CSI (0.1)	CSI (10)
0%	0.318	0.083
25%	<b>0.347</b>	<b>0.093</b>
50%	0.322	0.086

### D.2 Ablation study on lead time

In this section, the precipitation data of the NWP model was extracted and trained by extracting 25 to 30 forecasts to post-process with a 24 hour lead time. In the case of training, the lead time was not considered, and the accuracy was measured as shown in Figure 3 to understand the degree of CSI improvement by lead time. The results in Figure 4 show that the overall precipitation data was corrected regardless of the leading time, and the improvement was about 39.49% for the 27-hour forecast data. The results show that the proposed model is effective for precipitation correction and is robust to error correction due to lead time.

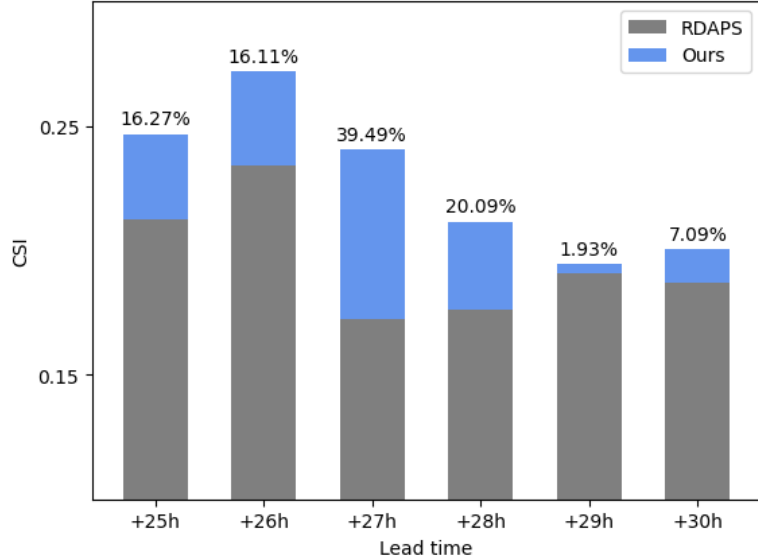


Figure 4: Bar plots by lead time. Scores with a CSI of 0.1 or higher and scores with a CSI of 10 or higher are averaged across lead times, and the improvement over RDAPS is shown in percentage.

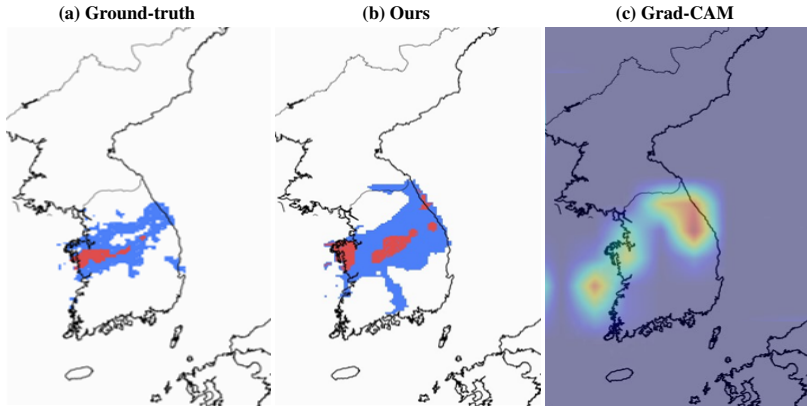


Figure 5: Heat map visualization at the depth selected for the test case: (a) Ground truth data; (b) segmented results; (c) heat map superimposed on top of the original image. In GradCAM maps, warmer colors indicate a higher pixel contribution to the correct prediction, while cooler colors signify a lower contribution.

### D.3 Marking Points of Interest

Zhou et al. [26] proposed a methodology for computing class-discriminative activation maps by employing a novel set of weights separately trained for each feature map in the context of image classification tasks. The class activation map is obtained by

$$M_{i,j}^c = \sum_{k=1} \omega_k^c m_{i,j}^k \quad (3)$$

where  $m_k$  is the  $k$ -th feature map of the final convolution layer, and the weights  $\omega_k^c$  are trained separately with global average pooling with individual feature maps  $F_k = \sum_i \sum_j m_{i,j}^k$ . The score of the class  $S_c$  is the sum over all class activation maps  $S_c = \sum_i \sum_j M_{i,j}^c$ . Grad-CAM [19] is a natural progression of the original CAM implementation, removing the necessity to train a fresh set

of weights. Instead the weight  $\omega_k^c$  for a certain class  $c$  can be calculated with

$$\omega_k^c = \sum_i \sum_j \frac{\partial S^c}{\partial m_{i,j}^k} \quad (4)$$

Fig. 5 shows a heatmap of the parts of the visualization that the model focuses on, based on the case compared in Fig. 3.